# Effects of Coulomb blockade on the photocurrent in quantum dot infrared photodetectors

David M.-T. Kuo and Yia-Chung Chang
*Department of Physics and Materials Research Laboratory, University of Illinois at Urbana-Champaign, Urbana, Illinois 61801*
(Received 14 August 2002; revised manuscript received 6 November 2002; published 16 January 2003)

We present theoretical studies of the effects of Coulomb blockade on the photocurrent of quantum dot infrared photodetectors within the Anderson model with two localized levels coupled with the electromagnetic field. We use the Keldysh Green function method to calculate the photocurrent. The energy levels, on-site Coulomb energy, and coupling parameters between leads and quantum dot states, as functions of the applied field, are evaluated within an effective mass model. It is found that the Coulomb interaction and level mixing in the many-body open system lead to a double-peak spectrum for the intraband transition. The center of gravity of the spectrum is redshifted as the applied bias increases, which competes with the blueshift caused by the Stark effect. Furthermore, the photocurrent is found to be a nonlinear function of the steady-state electron density of the quantum dot, in sharp contrast to quantum well infrared photo-detectors.

DOI: 10.1103/PhysRevB.67.035313 PACS number(s): 72.40.+w, 73.23.Hk, 73.63.Kv

## I. INTRODUCTION

Modern advanced techniques such as molecular beam epitaxy and metal-organic chemical-vapor deposition coupled with *e*-beam lithography can provide a good control of the size and shape of components in semiconductor circuits down to the nanometer scale, where the quantum effect becomes important. The interplay of quantum confinement and electron correlation leads to intriguing effects such as Coulomb blockade, conductance, fluctuation, and dephasing.[1] Recently, many efforts have been devoted to the understanding of transport properties in quantum dot nanostructures.[2–4] Quantum dot (QD) based systems have potential applications in optoelectronic devices, such as infrared detectors,[5,6] single photondetectors,[7] semiconductor lasers[8] and quantum computing.[9] In this paper our main purpose is to study the effect of electron correlation on the photocurrent of quantum dot infrared photo-detectors (QDIPs). The advantage of the QDIP over QWIP is that light can be directly coupled to the electrons in the normal incidence geometry due to the effect of QD confinement in directions perpendicular to the growth axis and the dark current is smaller for the same detection wave length considered.[5] Other significant features that are unique to QDs include the Coulomb blockade effect[6] and phonon bottleneck.[10]

Due to the localized nature of electrons in QDs, it is essential to take into account the effects of Coulomb blockade in the analysis of photoresponse of QDIPs, which in general can be ignored in QWIPs. For the nonequilibrium system considered here, it is convenient to use the Keldysh Green function to calculate the transport and optical properties while including the electron correlation. This technique has been used extensively in the study of nonlinear transport properties of quantum systems.[11–14] The tunneling current through quantum dots under microwave radiation has been studied by many authors via the Keldysh method[11–14] and the density matrix method.[15] In these studies, the electron-photon interaction is strong and the effect of electron correlation was ignored in order to avoid solving the time-dependent electron density in QD. The main emphasis of these studies was on multi-photon-assisted tunneling current, since the frequency of interest is much smaller than the electron Coulomb energy in the QD.

For the infrared absorption process in QDIPs considered here, the electron-photon coupling is fairly weak. Therefore, we only focus on the one-photon-assisted tunneling process as follows. Our main findings are:

(1) Electron correlation has a significant effect (Coulomb blockade) on the photoresponse of QDIPs. As a result of electron correlation, the photocurrent spectrum displays double peaks. In the case of large size fluctuation, the double peaks may be difficult to resolve, but the center of gravity of the spectrum will be red-shifted as the bias increases.

(2) The *I*-*V* characteristics of the photocurrent displays a steplike feature due to Coulomb blockade.

(3) Photocurrent in QDIPs is a highly nonlinear function of the steady-state carrier density in the QD unlike that in QWIPs.

## II. GENERAL FORMALISM

We start with the Hamiltonian $H$ within the rotating wave approximation (RWA)[16]

$$H=\sum_{\mathbf{k},\sigma}\epsilon_{\mathbf{k}}C^{\dagger}_{\mathbf{k},\sigma}C_{\mathbf{k},\sigma}+\sum_{\mathbf{p},\sigma}\epsilon_{\mathbf{p}}C^{\dagger}_{\mathbf{p},\sigma}C_{\mathbf{p},\sigma}+\sum_{i,\mathbf{k},\sigma}V_{i,\mathbf{k}}C^{\dagger}_{\mathbf{k},\sigma}d_{i,\sigma}+\mathrm{H.c.}+\sum_{i,\mathbf{p},\sigma}V_{i,\mathbf{p}}C^{\dagger}_{\mathbf{p},\sigma}d_{i,\sigma}+\mathrm{H.c.}+\sum_{i,\sigma}E_i d^{\dagger}_{i,\sigma}d_{i,\sigma}+\lambda\exp^{-i\omega t}d^{\dagger}_{2,\sigma}d_{1,\sigma}+\mathrm{H.c.}, \quad (1)$$

where the first two terms describe the left lead (emitter) and right lead (collector), respectively, the third and fourth term describe the coupling between the QD states and the two leads. Electron correlation in the two leads is ignored. We consider the situation where the QD contains two bound levels ($i=1,2$). The energy difference between two levels considered here is near 124 meV (for application in 10 $\mu$m wavelength detection). The last two terms describe the interaction of the QD electrons with incident photons. Because of

 

the RWA, only resonant terms are kept. Here $\omega$ is the frequency of the photons, while $\lambda$ is the matrix element for the optical transition

$$\lambda = \frac{e}{m^*\omega}\int \Psi_j(\mathbf{r})\mathbf{F}_t(\mathbf{r})\cdot\nabla\Psi_i(\mathbf{r})d\mathbf{r}, \tag{2}$$

where e and $m^*$ are the charge and the effective mass of electron, $\Psi_i(\mathbf{r})$ is the wave function of electrons in QD, and $F_t(\mathbf{r})$ is the strength of electromagnetic field. We have used the units such that $\hbar = c = 1$. This convention is used throughout this paper.

We introduce a unitary transformation $S(t)$,[15]

$$S(t) = \exp^{\frac{i\omega t}{2}(d^\dagger_{1,\sigma}d_{1,\sigma} - d^\dagger_{2,\sigma}d_{2,\sigma})}, \tag{3}$$

and define the transformed Hamiltonian by

$$H_{new} = S^\dagger(t)H(t)S(t) - S^\dagger(t)i\frac{\partial}{\partial t}S(t). \tag{4}$$

The Hamiltonian takes the form

$$\begin{aligned} H = &\sum_{\mathbf{k},\sigma} \epsilon_{\mathbf{k}} C^\dagger_{\mathbf{k},\sigma}C_{\mathbf{k},\sigma} + \sum_{\mathbf{p},\sigma} \epsilon_{\mathbf{p}} C^\dagger_{\mathbf{p},\sigma}C_{\mathbf{p},\sigma} + \sum_{i,\mathbf{k},\sigma} V_{i,\mathbf{k}}(t) C^\dagger_{\mathbf{k},\sigma}d_{i,\sigma} \\ &+ \text{H.c.} + \sum_{i,\mathbf{p},\sigma} V_{i,\mathbf{p}}(t) C^\dagger_{\mathbf{p},\sigma}d_{i,\sigma} + \text{H.c.} + \sum_{i,\sigma} \epsilon_i d^\dagger_{i,\sigma}d_{i,\sigma} \\ &+ \lambda d^\dagger_{2,\sigma}d_{1,\sigma} + \text{H.c.}, \end{aligned} \tag{5}$$

where the eigenstates of the QD are renormalized as $\epsilon_1 = E_1 + \omega/2$ and $\epsilon_2 = E_2 - \omega/2$. The total phase in the interlevel Hamiltonian vanishes. However ,the hopping terms are time dependent, $V_{j,\mathbf{k}}(t) = V_{j,\mathbf{k}}\exp^{-[(-1)^j i\omega/2]t}$ for $j = 1,2$, in which the energy and time dependence of the coupling are factorized. This factorization leads to time-independent tunneling rates and simplifies the calculation.

In small semiconductor QDs the effect of electron correlation is significant. We take into account the intralevel and interlevel Coulomb interactions by adding the following term to $H$:

$$\begin{aligned} H_I = &\sum_{i,\sigma} U_{ii} d^\dagger_{i,\sigma}d_{i,\sigma}d^\dagger_{i,-\sigma}d_{i,-\sigma} \\ &+ \sum_{i,\neq j;\sigma,\sigma'} U_{ij} d^\dagger_{i,\sigma}d_{i,\sigma}d^\dagger_{j,\sigma'}d_{j,\sigma'}. \end{aligned} \tag{6}$$

Both the interlevel Coulomb interaction $U_{12}(U_{21})$ and the intralevel Coulomb interaction in the ground state $U_{11}$ will modify the interlevel transition energy; thus they cannot be ignored, while the intralevel Coulomb interaction $U_{22}$ can be ignored since the electron population in the second level is negligibly small. The Coulomb interaction $H_I$ is invariant under the unitary transformation. We have extended the approach given by Jouho and co-workers[11,12] to the present case with asymmetric tunneling rates. We find that the time-averaged tunneling current is given by

$$\begin{aligned} \langle J(t)\rangle = &\sum_j (\Gamma^R_j - \Gamma^L_j)\frac{e\langle N_j(t)\rangle}{2} - e\,\text{Im}\sum_j \int \frac{d\epsilon}{\pi}[\Gamma^L{}_j f_L \\ &\times(\epsilon - \mu_L) - \Gamma^R{}_j f_R(\epsilon - \mu_R)]\langle u_j(t)\mathbf{A}_j(\epsilon,t)\rangle. \end{aligned} \tag{7}$$

In Eq. (7), $\langle N_j(t)\rangle$ is the electron occupation number at QD, $f_L(\epsilon - \mu_L)$ and $f_R(\epsilon - \mu_R)$ are the Fermi distribution function of the left lead and right lead, respectively. The chemical potential difference between these two leads is related to the applied bias (2 V) via $\mu_L - \mu_R = 2$ eV. $\Gamma^L_j$ and $\Gamma^R_j$ denote the tunneling rates from the QD to the left and right leads, respectively, for electrons in level $j$. The tunneling rates as functions of the energy and bias can be determined numerically once the confining potential for the QD is known.[5] The notation Im means "taking the imaginary part." The time average of $u_j(t)\mathbf{A}_j(\epsilon,t)$ with period T is defined by

$$\langle u_j(t)\mathbf{A}_j(\epsilon,t)\rangle = \frac{1}{T}\int_{-T/2}^{T/2} dt u_j(t)\mathbf{A}_j(\epsilon,t), \tag{8}$$

where $u_j(t) = e^{-(-1)^j(i\omega t/2)}$ and

$$A_j(\epsilon,t) = \int_{-\infty}^{t} dt_1 \exp^{i\epsilon(t-t_1)}u^*_j(t_1)G^r_{jj}(t,t_1). \tag{9}$$

$G^r_{ij;\sigma}(t_1,t_2) \equiv -i\theta(t_1 - t_2)\langle[d_{i,\sigma}(t_1), d^\dagger_{j,\sigma}(t_2)]_+\rangle$ is the retarded Green function of the QD. The diagonal elements of $G^r_{ij;\sigma}$ describe the propagation within the same QD level from time $t_2$ to point $t_1$. The off-diagonal elements describe the same propagation but with transition from level $j$ to level $i$. $\langle N_j(t)\rangle$ and $G^r_{ij,\sigma}(t,t_1)$ in Eq. (7) are the key ingredients for the tunneling current. To solve the above Green function, the tunneling process[11] and pumping process[17] must be included simultaneously. The first term in Eq. (7) for the excited state $(j = 2)$ provides the photoinduced tunneling current which exists only when $\Gamma^R_2 \neq \Gamma^L_2$, a condition that can occur in a system with asymmetric potential (i.e., with an internal electric field) such as the self-assembled QDs considered here or with applied bias.

## III. TUNNELING CURRENT

The calculation of tunneling current is entirely determined by the Green funtion of the QD. First we study the retarded Green function. Dyson's equation is introduced as

$$\begin{aligned} G^r_{ij,\sigma}(t,t_1) = &g^r_{ij;\sigma}(t,t_1) + \int dt_2 \int dt_3 g^r_{im;\sigma}(t,t_2) \\ &\times \Sigma^r_{m,n'}(t_2,t_3)G^r_{n'j;\sigma}(t_3,t_1), \end{aligned} \tag{10}$$

where $g^r_{ij;\sigma}(t,t') = -i\theta(t,t')\langle[d_{i,\sigma}(t), d^\dagger_{j,\sigma}(t')]_+\rangle$ is the retarded Green function without including electron-photon interaction and electron lead coupling. We can use the equations of motion to determine a approximate solutions of $g^r_{ij;\sigma}$:

$$\left(\frac{i\partial}{\partial t} - \epsilon_1\right)g^r_{11;\sigma}(t,t') = \delta(t - t') + U_{12}\mathcal{G}_{12} + U_{11}\mathcal{G}_{11} \tag{11}$$

and

$$\left(\frac{i\partial}{\partial t}-\epsilon_2\right)g^r_{22;\sigma}(t,t')=\delta(t-t')+U_{12}\mathcal{G}_{21}+U_{22}\mathcal{G}_{22}. \tag{12}$$

$\mathcal{G}_{ij}$ is a two particle Green function defined by $\mathcal{G}_{ij}=-i\theta(t-t')\langle[d_{i,\sigma}(t)d^\dagger_{j,\sigma'}(t)d_{j,\sigma'}(t),d^\dagger_{i,\sigma}(t')]_+\rangle$, where $\sigma'=-\sigma$. The constraint $\sigma'=-\sigma$ is caused by the Pauli exclusion principle for $i=j$ and by the spin conservation in the pumping process for $i\neq j$, since the electrons in the excited states are produced by the photoexcitation, not by injection from leads.

The equation of motion for $\mathcal{G}_{ij}$ are given by

$$\left(\frac{i\partial}{\partial t}-\epsilon_i-U_{ij}\right)\mathcal{G}_{ij}=\delta(t-t')n_{j,-\sigma}(t). \tag{13}$$

For $g^r_{11}$, we can ignore the effect of $\mathcal{G}_{12}$ because it is proportional to the electron occupation number in level 2, which is negligible. Consequently, we obtain

$$g^r_{11}(t,t_1)=-i\theta(t-t_1)[\exp^{-i\epsilon_1(t-t_1)}(1-N_1)+\exp^{-i(\epsilon_1+U_{11})(t-t_1)}N_1]. \tag{14}$$

Similarly, for $g^r_{22}$, we can ignore $\mathcal{G}_{22}$ (owing to the small electron occupation number in level 2), and obtain

$$g^r_{22}(t,t_1)=-i\theta(t-t_1)[\exp^{-i\epsilon_2(t-t_1)}(1-N_1)+\exp^{-i(\epsilon_2+U_{12})(t-t_1)}N_1]. \tag{15}$$

Off-diagonal Green functions $g^r_{12}$ and $g^r_{21}$ vanish. The spin indexes are omitted in Eqs. (14) and (15), since the Hamiltonian is spin independent. The Green functions $g^r_{11}$ and $g^r_{22}$ have two branches: one describes the one-particle propagation, the other describes the two-particle propagation. In addition we approximate the time dependent electron occupation number $N_1$ by its time averaged value. This is a good approximation for the weak electron-photon coupling case $[\lambda/\omega_r\ll 1\ (\omega_r\equiv E_2-E_1)]$ considered here.

Now let us consider the effect due to electron-photon coupling and the finite lifetime of the QD levels which are caused by the coupling with leads and other decaying processes. The retarded self-energy in Eq. (10) is given by

$$\Sigma^r=\begin{pmatrix}-i\Gamma_1/2 & \lambda\\ \lambda^* & -i\Gamma_2/2\end{pmatrix}\delta(t_2-t_3). \tag{16}$$

Introducing the Fourier transform (Ref. 18)

$$G^r_{ij}(t,t_1)=\sum_n \exp^{-in\omega t}\int\frac{d\varepsilon}{2\pi}\exp^{-i\varepsilon(t-t_1)}G^r_{ij,n}(\varepsilon), \tag{17}$$

where n is the photon number, for $\lambda/\omega_r\ll 1$ the "zero photon process" $(n=0)$ is dominant.[19] Therefore, only $G^r_{ij;0}$ is important. Substituting Eqs. (14)–(17) into Eq. (10), we obtain

$$G^r_{ii;0}(\varepsilon)=\frac{G^{r0}_{ii}(\varepsilon)}{1-\lambda^2G^{r0}_{11}(\varepsilon)G^{r0}_{22}(\varepsilon)} \tag{18}$$

and

$$G^r_{12,0}(\varepsilon)=G^r_{21,0}(\varepsilon)=\frac{\lambda G^{r0}_{11}(\varepsilon)G^{r0}_{22,\sigma}(\varepsilon)}{1-\lambda^2G^{r0}_{11}(\varepsilon)G^{r0}_{22}(\varepsilon)}, \tag{19}$$

with

$$G^{r0}_{11}(\varepsilon)=\frac{g^r_{11}(\varepsilon)}{1-g^r_{11}(\varepsilon)(-i\Gamma_1/2)}\approx\frac{1-N_1}{\varepsilon-\epsilon_1+i\Gamma_1/2}+\frac{N_1}{\varepsilon-\epsilon_1-U_{11}+i\Gamma_1/2} \tag{20}$$

and

$$G^{r0}_{22}(\varepsilon)=\frac{g^r_{22}(\varepsilon)}{1-g^r_{22}(\varepsilon)(-i\Gamma_2/2)}\approx\frac{1-N_1}{\varepsilon-\epsilon_2+i\Gamma_2/2}+\frac{N_1}{\varepsilon-\epsilon_2-U_{12}+i\Gamma_2/2}, \tag{21}$$

where

$$g^r_{11}(\varepsilon)=\frac{1-N_1}{\varepsilon-\epsilon_1}+\frac{N_1}{\varepsilon-\epsilon_1-U_{11}}, \tag{22}$$

and

$$g^r_{22}(\varepsilon)=\frac{1-N_1}{\varepsilon-\epsilon_2}+\frac{N_1}{\varepsilon-\epsilon_2-U_{12}}. \tag{23}$$

Our results [Eqs. (18) and (19)] can be mapped into the coupled QD problems considered by You and Zheng.[20] They derived results similar to our Eqs. (18) and (19) via different approximations.[20] The role of $\lambda$ here is analogous to the interdot hopping term in their coupled QD problem. Before we solve $N_j$, let us consider the noninteracting case by setting $U_{11}=U_{12}=0$ in Eq. (18). The poles of Eq. (18) are $[E_1+E_2\pm\sqrt{(E_2-E_1-\omega)^2+4\lambda^2}]/2$. This result is the same as that of Ref. 15, where a two-level system without electron correlation under the microwave radiation was studied.

To calculate the electron occupation number of the QD, we need to introduce the lesser Green function $G^<_{ij}(t_1,t_2)=i\langle d^\dagger_j(t_2)d_i(t_1)\rangle$ which describes the correlation of electrons in energy levels $i$ and $j$ at times $t_1$ and $t_2$. The equation of motion of $G^<_{ij}(t_1,t_2)$ is given by

$$\left(i\frac{\partial}{\partial t}-\epsilon_i+\epsilon_j\right)G^<_{i,j,\sigma}(t_1,t_2)=\Sigma^r_{i,l}(t_1,t_3)G^<_{l,j,\sigma}(t_3,t_2)$$
$$-G^<_{i,l,\sigma}(t_1,t_3)\Sigma^a_{l,j}(t_3,t_2)$$
$$-G^r_{i,l,\sigma}(t_1,t_3)\Sigma^<_{l,j}(t_3,t_2)$$
$$+\Sigma^<_{i,l}(t_1,t_3)G^a_{l,j,\sigma}(t_3,t_2)$$
$$+(1-\delta_{i,j})\mathcal{T}^<_{ij,\sigma}(t_1,t_2) \tag{24}$$

where $G^a$ denotes the advanced Green function, and $t=(t_1+t_2)/2$. $\Sigma^r$, $\Sigma^a$, and $\Sigma^<$ are the retarded, advanced, and lesser self-energy, respectively. The last term (which is nonzero only for $i\neq j$ and valid under the condition $N_2\ll N_1$) describes the coupling to the two-particle ''lesser'' Green functions $\mathcal{G}^<_{12,\sigma}$ and $\mathcal{G}^<_{21,\sigma}$:

$$\mathcal{T}^<_{12,\sigma}(t_1,t_2)=U_{11}i\langle d^\dagger_{2,\sigma}(t_2)n_{1,-\sigma}(t_1)d_{1,\sigma}(t_1)\rangle$$
$$-U_{12}i\langle n_{1,-\sigma}(t_2)d^\dagger_{2,\sigma}(t_2)d_{1,\sigma}(t_1)\rangle,$$
$$=U_{11}\mathcal{G}^<_{12,\sigma}(t_1,t_2)-U_{12}\overline{\mathcal{G}^<_{12,\sigma}}(t_1,t_2)$$

and

$$\mathcal{T}^<_{21,\sigma}(t_1,t_2)=-U_{11}i\langle n_{1,-\sigma}(t_2)d^\dagger_{1,\sigma}(t_2)d_{2,\sigma}(t_1)\rangle$$
$$+U_{12}i\langle d^\dagger_{1,\sigma}(t_2)n_{1,-\sigma}(t_1)d_{2,\sigma}(t_1)\rangle.$$

$\mathcal{G}^<_{12,\sigma}(t_1,t_2)(\mathcal{G}^<_{21,\sigma}(t_1,t_2))$ can be determined by an equation of motion. The self-energies of Eq. (24) are given by

$$\Sigma^{r(a)}(t',t'')=\begin{pmatrix}\mp i\Gamma_1/2 & \lambda\\ \lambda^* & \mp i\Gamma_2/2\end{pmatrix}\delta(t'-t'') \tag{25}$$

and

$$\Sigma^<(t',t'')=i\int\frac{d\epsilon}{2\pi}[\Gamma^L_j f_L(\epsilon)$$
$$+\Gamma^R_j f_R(\epsilon)]\exp^{-i\epsilon(t'-t'')}u^*_j(t')u_j(t''). \tag{26}$$

The electron occupation number $N_{j,\sigma}$, now, can be obtained from the equal-time lesser Green function $G^<_{ij,\sigma}(t_1,t_1)$. Substituting Eqs. (25), and (26) into Eq. (24), we obtain the following set of rate equations (omitting the higher order terms in $\lambda$):

$$\left\langle i\frac{\partial}{\partial t}N_1(t)\right\rangle=-i\Gamma_1N_1-2\,\mathrm{Im}(\lambda^*p)$$
$$-\int\frac{d\epsilon}{\pi}\Gamma^{L/R}_1 f_{L/R}(\epsilon)\,\mathrm{Im}\,G^r_{11,0}\left(\epsilon+\frac{\omega}{2}\right), \tag{27}$$

$$\left\langle i\frac{\partial}{\partial t}N_2(t)\right\rangle=-i\Gamma_2N_2+2\,\mathrm{Im}(\lambda^*p)$$
$$-\int\frac{d\epsilon}{\pi}\Gamma^{L/R}_2 f_{L/R}(\epsilon)\,\mathrm{Im}\,G^r_{22,0}\left(\epsilon-\frac{\omega}{2}\right), \tag{28}$$

$$\left\langle i\frac{\partial}{\partial t}p(t)\right\rangle\approx\left[-i\left(\frac{\Gamma_1+\Gamma_2}{2}\right)+\epsilon_1-\epsilon_2\right]p-\lambda(N_1-N_2)$$
$$+(U_{11}-U_{12})\langle-i\mathcal{G}^<_{12}(t,t)\rangle, \tag{29}$$

$$\left\langle i\frac{\partial}{\partial t}\mathcal{G}^<_{12}(t,t)\right\rangle\approx\left[-i\left(\frac{\Gamma_1+\Gamma_2}{2}\right)+\epsilon_1-\epsilon_2-U_{12}+U_{11}\right]$$
$$\times\langle\mathcal{G}^<_{12}(t,t)\rangle-i\lambda(N_1-N_2)N_1, \tag{30}$$

where $N_{ii}=\langle-iG^<_{ii}(t,t)\rangle$ and $p_{i,j}=\langle-iG^<_{ij}(t,t)\rangle$ are time-averaged diagonal and nondiagonal elements of the lesser Green function. We have ignored the spin index in Eqs. (27)–(30), since $H$ is spin independent. The last term of right sides of Eqs. (27) and (28) represents the electron injection rates from the leads.

Imposing the steady state conditions $\langle\partial N/\partial t\rangle=0$ and $\langle\partial p/\partial t\rangle=0$, we obtain

$$\Gamma_1N_1=-\,\mathrm{Im}\,\mathcal{X}(\omega)-\int\frac{d\epsilon}{\pi}[\Gamma^L_1f_L(\epsilon)+\Gamma^R_1f_R(\epsilon)]$$
$$\times\,\mathrm{Im}\,G^r_{11,0}\left(\epsilon+\frac{\omega}{2}\right),$$
$$\Gamma_2N_2=\mathrm{Im}\,\mathcal{X}(\omega)-\int\frac{d\epsilon}{\pi}[\Gamma^L_2f_L(\epsilon)+\Gamma^R_2f_R(\epsilon)] \tag{31}$$
$$\times\,\mathrm{Im}\,G^r_{22,0}\left(\epsilon-\frac{\omega}{2}\right),$$

and

$$\mathcal{X}(\omega)=2\lambda^*p=2\lambda^2(N_2-N_1)\left\{\frac{1-N_1}{\epsilon_2-\epsilon_1+i\dfrac{\Gamma_1+\Gamma_2}{2}}\right.$$
$$\left.+\frac{N_1}{\epsilon_2-\epsilon_1+U_{12}-U_{11}+i\dfrac{\Gamma_1+\Gamma_2}{2}}\right\}, \tag{32}$$

$\mathrm{Im}\,\mathcal{X}(\omega)$ determines the line-shape of the photocurrent. $\mathcal{X}(\omega)$ has two poles at the resonant frequencies $\omega_r=E_2-E_1$ and $\omega_{r1}=E_2-E_1+U_{12}-U_{11}$, respectively. They correspond to the interlevel optical transition of an electron with or without the influence of the Coulomb repulsion with another electron (of opposite spin) which remains in level 1 during the transition. Since $U_{12}$ is always less than $U_{11}$, this leads to a redshift in the second term with respect to the first term. For an open system, the average steady-state occupancy in level 1 (for a given spin) can very between 0 and 1,

depending on the bias. Thus we obtain a splitting in transition peaks due to the electron-electron correlation.

It is instructive to note that if one adopts the Hartree approximation, the number operator $n_{1,\sigma}$ which appears in $\mathcal{G}_{12}^{<}$ can be replaced by $N_1$, and $-i\mathcal{G}_{12}^{<}$ in Eq. (29) reduces to $N_1 p$. Consequently, $\mathcal{X}(\omega)$ reduces to the simplified form

$$\mathcal{X}(\omega)=\frac{2\lambda^2(N_2-N_1)}{\epsilon_2-\epsilon_1+N_1(U_{12}-U_{11})+i\dfrac{\Gamma_1+\Gamma_2}{2}}. \tag{33}$$

This leads to single-peak spectrum with the peak position corresponding to the weighted average of the two-peak spectrum given in Eq. (32). For QDIP systems with large size fluctuations, the broadening in the spectrum can be larger than the energy splitting $U_1-U_{12}$. In this case the line shape obtained from the Hartree approximation becomes similar to that obtained by using Eq. (32).

To obtain the average steady-state occupancy in level $j(N_j)$, we must solve Eqs. (31) and (32) self-consistently. In the limit of weak electron-photon coupling considered here, we can ignore the $\lambda^2$ term and obtain $G_{ii,0}^{r}\approx G_{ii,\sigma}^{r0}$ [see Eq. (18)]. For the ground state, $G_{11,\sigma}^{r0}$ consists of two poles with weighting factors $1-N_1$ and $N_1$ [see Eq. (20)]. Physically, this means that an electron once placed in level $i=1$ can propagate either though an empty QD (with probability $1-N_1$) or an occupied QD (with probability $N_1$). When the chemical potential $\mu_L$ is above $E_1$, but below $E_1+U_{11}$, $N_1$ (for a fixed spin) as a function of bias will display a plateau. Only when $\mu_L$ is above $E_1+U_{11}$ (i.e., when the bias overcomes the Coulomb repulsion caused by the electron originally residing at the QD), the electron number at the QD increase again with the increasing bias. This is the well-known Coulomb-blockade effect.[11]

Finally we write the time averaged tunneling current through the energy level j as

$$\langle J(t)_j\rangle=(\Gamma_j^R-\Gamma_j^L)\frac{e\langle N_j(t)\rangle}{2}-e\int\frac{d\epsilon}{\pi}[\Gamma_j^L f_L(\epsilon)-\Gamma_j^R f_R(\epsilon)]\,\mathrm{Im}\,G_{jj,0}^{r}\left(\epsilon-(-1)^j\frac{\omega}{2}\right). \tag{34}$$

Equations (31)–(34) are the central results of this article.

## IV. APPLICATION TO SELF-ASSEMBLED QDS

We now apply our theory to a realistic self-assembled quantum dot (SAQD) device. We consider an In-GaAs/GaAs SAQD system with conical shape (see Fig. 1). The SAQD is embedded in a slab of GaAs with a finite width *W*. The slab is then placed in contact with heavily doped GaAs to form an *n-i-n* structure for infrared detection. Within the effective-mass model,[5] the QD electron is described by the equation

$$\left[-\nabla\frac{1}{2m^*(\rho,z)}\nabla+V(\rho,z)-eFz\right]\psi(\rho,\phi,z)=E\psi(\rho,\phi,z).$$

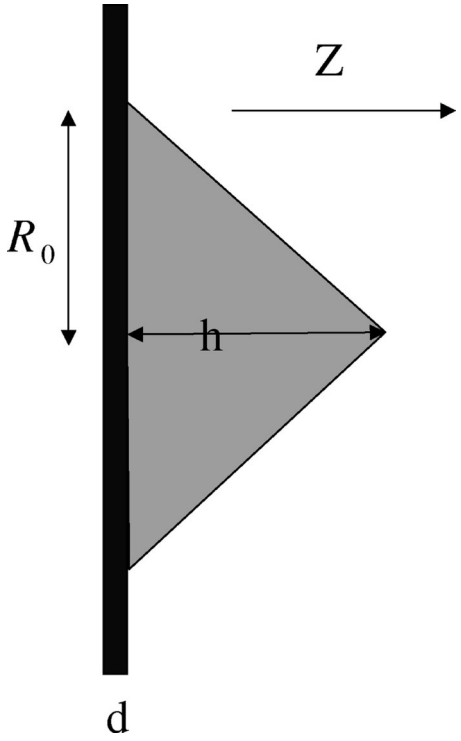


FIG. 1. Schematic diagram for a conical InGaAs/GaAs quantum dot.

$m^*(\rho,z)$ is the position-dependent effective mass, which takes on values of $m_G^*=0.067m_e$ (for GaAs) and $m_I^*=0.024m_e$ (for InAs). The potential $V(\rho,z)$ is equal to 0 in the GaAs barrier region and $V_0$ inside the InGaAs QD region. The potential in the depletion layers (which separate the slab from the leads) are modeled by an electrostatic potential

$$V_d(z)=\begin{cases}\dfrac{-V_1}{D}(z+W/2) & \text{for} \quad -(D+W/2)<z<-W/2\\ \dfrac{V_1}{D}(z-W/2) & \text{for} \quad W/2<z<D+W/2.\end{cases}$$

The potential profile along the *z* axis for the QDIP structure is depicted in Fig. 2.

For the purpose of constructing the approximate wave functions, we place the system in a large cylindrical confining box with length *L* and radius $R$($R$ must be much larger than the radius of the cone, $r_c$). In this paper we adopt $R=400$ Å, $D=350$ Å, $V_1=-0.205$ eV, and $W=300$ Å for all calculations. We solve the eigenfunctions of the effective-

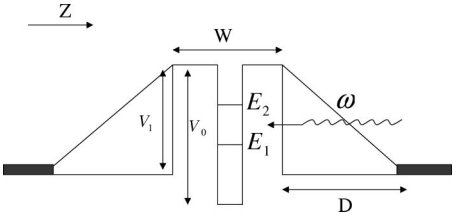


FIG. 2. Potential profile along the *z* axis for the QDIP.

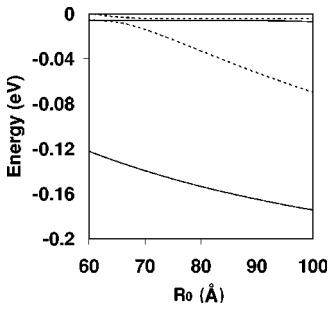


FIG. 3. Energies of the bound states of a conical $In_{0.2}Ga_{0.8}As/GaAs$ QD as functions of the base radius $R_0$ of the QD with height fixed at $h=50$ Å. Solid lines: $(l=0)$. Dotted lines: $(l=1)$.

mass Hamiltonian via the Ritz variational method. The wave functions are expanded in a set of basis functions which are chosen to be products of Bessel functions and sine waves

$$\psi_{nlm}(\rho,\phi,z)=J_l(\alpha_n\rho)e^{il\phi}\sin\left[k_m\left(z+\frac{L}{2}\right)\right],$$

where $k_m=m\pi/L, m=1,2,3,\ldots$. Throughout this paper, the origin of z is set at the middle of the confining box. $J_l$ is the Bessel function of order $l(l=0,1,2,\ldots,$ etc.) and $\alpha_n R$ is the $n$th zero of $J_l(x)$. 40 sine functions multiplied by 15 Bessel functions for each angular function ($l=0$ or 1) are used to diagonalize the Hamiltonian. The convergence is checked by increasing the basis functions and with the current set of basis the ground state energy is accurate to within 1 meV.

Figure 3 shows the energy levels of the confined states with $l=0$ (solid line) and 1 (dotted line) as a function of the base radius $R_0$ of the QD with height fixed at $h=50$ Å. The other material parameters used here are: wetting layer thickness $d=3$ Å, the conduction-band offset $V_0=-0.4$ eV (this includes the effect of hydrostatic strain due to the lattice mismatch between $In_{0.2}Ga_{0.8}As$ and GaAs), and length of the confining box $L=600$ Å. At least two bound states for each angular function ($l=0$ or 1) are found. For infrared detector application, we are seeking an intraband transition (between the ground and first excited states) at a energy around 0.125 eV, which occurs at $h=50$ Å for $R_0=70$ Å.

The tunneling rates can be calculated numerically via the stabilization method as described in Ref. 5. Under zero bias, the tunneling rates $\Gamma_j^R(\Gamma_j^L)$ are calculated by replacing the left (right) half of the potential with a constant potential $V=0$, so that the electron is allowed to tunnel only to the right (left). For positive bias, $\Gamma_j^L$ are negligibly small, and there is no need to put additional constraint.

## V. RESULTS AND DISCUSSION

For photon frequency $\omega$ at the the resonance frequency $\omega_r=E_2-E_1$ and without the Coulomb interaction ($U_{11}=U_{12}=0$), the retarded Green function $G^r_{jj,0}$ in Eq. (34) contains poles located at $E_1\pm\lambda$ and $E_2\pm\lambda$. This is caused by the optical Stark effect,[18] which can be ignored for the weak electron-photon coupling considered here. The optical Stark effect for a quantum well system with strong electron photon coupling was studied by Johansson and Wendin.[18] Note that the retarded Green function given in Eq. (18) for the non-interacting case is exactly the same as Eq. (30) of Ref. 18. When $\omega$ is far from $\omega_r$, $G^r_{ii,0}$ contains four poles at $E_1$, $E_1+\omega$, $E_2$, and $E_2-\omega$. Note that the electron tunneling occurs as the chemical potential $\mu_{L/R}$ sweep through these poles (resonance energies). Although poles $E_1+\omega$ and $E_2-\omega$ can provide tunneling current (via the photon-assisted tunneling process), their contribution is negligibly small for the weak electron-photon coupling considered here. This is easy to check via numerical method. Consequently, we will not consider the nonresonant photon-assisted tunneling current in the following discussions.

Because of small $\lambda$ ($\lambda/\omega\ll 1$). $G^r_{ii,0}(\varepsilon)\approx G^{r0}_{ii,\sigma}(\varepsilon)$, which means that we can ignore the photon renormalization in the tunneling process, but not in the pumping process. We will only consider the low-bias case, where the chemical potential of leads ($\mu_L$ and $\mu_R$) is lower than $E_2$, so that the average population in the excited state remains small. Using Eqs. (31) and considering zero temperature, we obtain

$$N_2=N_1\frac{F(N_1)}{1+F(N_1)}=N_1\Lambda(N_1), \tag{35}$$

with

$$F(N_1)=-\frac{2\lambda^2}{\Gamma_2'}\mathrm{Im}\left\{\frac{1-N_1}{\epsilon_2-\epsilon_1+i\dfrac{\Gamma_1'+\Gamma_2'}{2}}+\frac{N_1}{\epsilon_2-\epsilon_1+U_{12}-U_{11}+i\dfrac{\Gamma_1'+\Gamma_2'}{2}}\right\}, \tag{36}$$

$N_1$ satisfies

$$N_1=\frac{-\Gamma_2'}{\Gamma_1'}N_1\Lambda(N_1)+\frac{1}{2\pi}\{(1-N_1)(F_1+F_3)+N_1(F_2+F_4)\}, \tag{37}$$

where

$$F_1=\tan^{-1}\left(\frac{V_a+E_F-E_1}{\Gamma_1'/2}\right)-\tan^{-1}\left(\frac{V_a-E_1}{\Gamma_1'/2}\right),$$

$$F_2=\tan^{-1}\left(\frac{V_a+E_F-E_1-U_{11}}{\Gamma_1'/2}\right)-\tan^{-1}\left(\frac{V_a-E_1-U_{11}}{\Gamma_1'/2}\right),$$

$$F_3=\tan^{-1}\left(\frac{-V_a+E_F-E_1}{\Gamma_1'/2}\right)-\tan^{-1}\left(\frac{-V_a-E_1}{\Gamma_1'/2}\right),$$

and

$$F_4 = \tan^{-1}\left(\frac{-V_a + E_F - E_1 - U_{11}}{\Gamma_1'/2}\right) - \tan^{-1}\left(\frac{-V_a - E_1 - U_{11}}{\Gamma_1'/2}\right).$$

Note that we have used $\Gamma_2' = \Gamma_2 + \Gamma_{2e}$ and $\Gamma_1' = \Gamma_1 + \Gamma_{1e}$ to replace $\Gamma_2$ and $\Gamma_1$ (tunneling rates). The broadening of the ground and the first excited state of Eq. (31) only considered the effect due to the QD coupling to the leads. For realistic systems, decaying processes other than the tunneling should be taken into account. Therefore , we add artificial terms $\Gamma_{2e}$ and $\Gamma_{1e}$ to include effects not considered in Hamiltonian [Eq. (1)]. At zero temperature, we obtain [according to Eq. (34)]

$$\langle J_1(t)\rangle = \frac{e\Gamma_1}{\pi}\{[(1-N_1)(F_1-F_3)+N_1(F_2-F_4)]\} \tag{38}$$

and

$$\langle J_2(t)\rangle = \frac{e(\Gamma_2^R - \Gamma_2^L)}{2}N_2 \sim \frac{e\Gamma_2^R}{2}N_2. \tag{39}$$

$\langle J_1(t)\rangle$ is determined solely by the spectral function $G^{r0}_{11,\sigma}$, and it gives rise to the dark current due to direct tunneling process. It displays the typical Coulomb blockade behavior. At very low temperatures (or high fields) the direct tunneling current is the dominant dark current.[21] $J \equiv \langle J_2(t)\rangle$ is the photocurrent, since $N_2$ is generated by the optical pumping process. From Eqs. (39) and (35) we see that the photocurrent is a nonlinear function of $N_1$. This is in sharp contrast with QWIP device, in which the Coulomb interaction can be neglected, and the photocurrent is linearly proportional to $N_1$.

Depending on the chemical potential of the leads, the zero-bias average electron occupancy per spin channel in the QD ground state can be either 0 (unfilled), 0.5 (half filled), or 1 (completely filled). Let us first consider the unfilled case. In this case, the Fermi level in the leads is below the QD ground state level. However, as we increase the bias such that the QD ground state level becomes charged, and a photocurrent can be detected.

Figures 4 and 5 show the photocurrent as a function of frequency for various voltages: $V_a = 0.11$ V (solid line), $V_a = 0.12$ V (dotted line), and $V_a = 0.13$ V (dashed line). The parameters used in these plots are $E_1 = -139$ meV, $E_2 = -14$ meV, $U_{11} = 10.4$ meV, and $U_{12} = 7.2$ meV, which are all calculated based on the effective-mass model described in the previous section. The Fermi level in the source and drain region is assumed to $E_F = 15$ meV. The broadening of the energy level $E_1$ including all tunneling processes (dominated by the acoustic-phonon assisted tunneling in this case) is assumed to be $\Gamma_1' = 0.01$ meV. The precise value of $\Gamma_1'$ is not important, since photocurrent is not sensitive to $\Gamma_1'$. In realistic samples, $\Gamma_{2e}$ is mainly due to radiative and nonradiative recombinations from interacting with phonons and defects. In addition, the broadening of the tunneling spectrum due to the quantum dot size fluctuation can also be included into

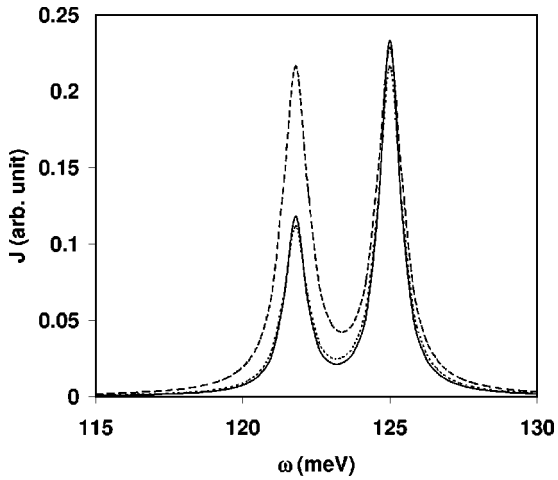


FIG. 4. Photocurrent as a function of frequency for various applied voltages: $V_a = 0.11$ V (solid line), $V_a = 0.12$ V (dotted line), and $V_a = 0.13$ V (dashed line). Low doping case ($E_F = 15$ meV) and $\Gamma_{2e} = 0.1$ meV.

$\Gamma_{2e}$. The actual value depends on the sample quality and temperature. We consider two extreme cases with $\Gamma_{2e} = 0.1$ meV (for an isolated QD) in Fig. 4 and 3 meV (for a system with a distribution of QDs of different sizes) in Fig. 5. The other contribution due to the direct tunneling is calculated via the stabilization method as described in Ref. 5. The values are found to be $\Gamma_2^R = 0.439$, 0.545, and 0.651 meV for $V_a = 0.11$, 0.12, and 0.13 V, respectively. The electron-photon coupling can be calculated from Eq. (2). In our case we consider the normal incident light (with in-plane polarization). Due to the lateral quantum confinement, the normal incident light can be directly coupled with the intraband electronic excitations in conical QDs. This is one of the most important advantage of QD infrared detector.

As shown in Fig. 4, the Coulomb interaction leads to a double-peak photocurrent spectrum with energy separation

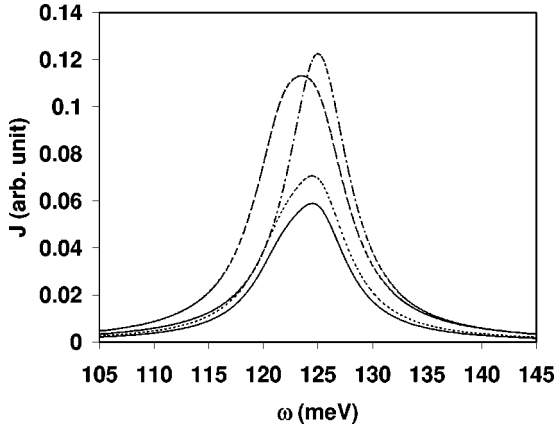


FIG. 5. Photocurrent as a function of frequency for various applied voltages: $V_a = 0.11$ V (solid line), $V_a = 0.12$ V (dotted line), $V_a = 0.13$ V (dashed line). Low doping case ($E_F = 15$ meV) and $\Gamma_{2e} = 3$ meV. Also included for comparison is the photocurrent spectrum without Coulomb interaction at $V_a = 0.12$ V (dot-dashed line).

equal to the difference in the intralevel and interlevel Coulomb energies ($U_{11}-U_{12}$). The high frequency peak corresponds to the interlevel transition [with relative probability $(1-N_1)$] of a single electron in the QD , while the low-frequency peak corresponds to the interlevel transition [with a relative probability $N_1$] of a second electron in the QD under the influence of the first electron, which remains in the ground state at all times. The relative strength of these peaks are determined by the average occupation number in the ground state $N_1$, which is bias dependent. For $\omega=\omega_r=E_2-E_1$, the photocurrent at $V_a=0.12$ V is smaller than that at $V_a=0.11$ V. This is because the photocurrent is proportional to $\Gamma_2^R(1-N_1)N_1/(\Gamma_2')^2$, which approximately equals $(1-N_1)N_1/\Gamma_2^R$ for the case $\Gamma_{2e}<\Gamma_2^R$ considered here. For $\omega=\omega_r+U_{12}-U_{11}$, the photocurrent is proportional to $\Gamma_2^R N_1^2/(\Gamma_2')^2\approx N_1^2/\Gamma_2^R$. Note that $N_1\approx 0.3$ for $V_a=0.11$ and 0.12 V, and $N_1\approx 0.5$ for $V_a=0.13$ V. Thus, the low-frequency peak has a big jump as $V_a$ changes from 0.12 to 0.13 due to the factor $N_1^2$.

For the case with a large QD size fluctuation, the photocurrent spectrum can be broadened substantially as shown in Fig. 5 for $\Gamma_{2e}=3$ meV. Also included for comparison in Fig. 5 is the photocurrent at $V_a=0.12$ V without the Coulomb interaction (dot-dashed line). As a result of the inhomogeneous broadening, the two peaks merge into one, and the result becomes essentially the same as that obtained from the Hartree approximation [Eq. (33)]. The peak position of the (broadened) photocurrent spectrum shifts toward the low-frequency side with increasing bias. This redshift behavior is due to the increased weight of the low-frequency peak as the bias increase. This bias-dependent redshift can also be understood roughly by examining the pole of Im $\mathcal{X}$ obtained in the Hartree approximation, which occurs at $\omega=\omega_r-(U_{11}-U_{21})N_1$, while $N_1$ increases with the bias. The Stark shift for energy levels has been excluded in Fig. 5 in order to illustrate the sole effect of the Coulomb interaction. The Stark effect leads to a blueshift in the transition energies, which competes with the redshift caused by the Coulomb interaction. At $V_a=0.11$, 0.12, and 0.13 V, the blueshifts due to the Stark effect are calculated (based on the effective-mass model described in Sec. IV) to be 1.35, 1.4, and 1.47 meV, respectively. The calculated photocurrent spectra, including both the Stark effect and Coulomb interaction display virtually no shift with peak positions at 125.6, 125.6, and 124.9 meV for $V_a=0.11$, 0.12, and 0.13 V, respectively.

For the QDIP characteristics, the photocurrent versus applied bias is also of interest.[22,23] Figure 6 shows the calculated photocurrent as a function of bias for $\Gamma_{2e}=0.1$ meV and $\Gamma_{2e}=3$ meV. In the former we consider two incident photon frequencies at $\omega_r$ (dotted line) and $\omega_r+U_{12}-U_{11}$ (solid line). In the latter, we only consider the incident photon frequency at $\omega_r$ (dashed line). Due to the inhomogeneous broadening, the photocurrent is substantially reduced. For better display, the value of the dashed line has been multiplied by a factor of 10. Using Eq. (32) for $\mathcal{X}(\omega)$, we can readily understand the behavior of the photocurrent. The photocurrent is proportional to the prefactor $(1-N_1)N_1$ at $\omega=\omega_r$ and $N_1^2$ at $\omega=\omega_r+U_{12}-U_{11}$. At low bias, $N_1$ is small; thus the magnitude of the solid line is much weaker than that of the dotted line. As the applied bias increases, the solid line displays a plateau due to the effect of Coulomb blockade on $N_1$. When the applied bias overcomes the charging effect, $N_1\approx 0.5$ and the solid line becomes almost identical to the dotted line.

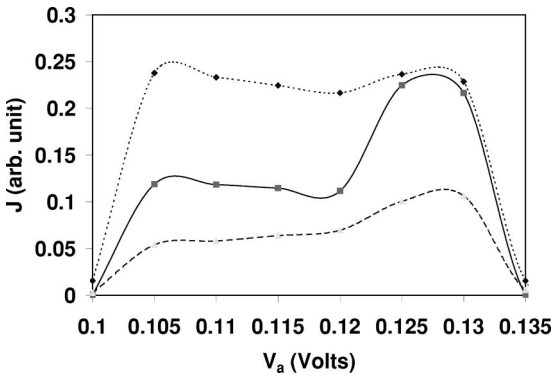


FIG. 6. Photocurrent as a function of bias for incident frequencies at $\omega=E_2-E_1$ (dotted line) and $\omega=E_2-E_1+U_{12}-U_{11}$ (solid line) and $\Gamma_{2e}=0.1$ meV. The dashed line denotes the photocurrent as a function of bias for incident frequency at $\omega=E_2-E_1$ and $\Gamma_{2e}=3$ meV.

Next we consider the high doping case. In this case, the Fermi level is above the QD ground state level, but not high enough to overcome the intralevel Coulomb repulsion, $U_{11}$. At very low bias, the dark current is blockaded due to Pauli exclusion principle. However, the photocurrent can still exist even at zero bias, due to the asymmetric tunneling rates. This can lead to high detectivity due to the large photocurrent -to-dark current ratio.[25] Figure 7 shows the calculated photocurrent spectra for the same QDIP structure as considered in Fig. 4, except that the Fermi level in the leads is now 70 meV. In Fig. 7, $V_a=0$ (solid line), [$V_a=0.11$ V (dotted line), $V_a=0.12$ V (dashed line), and $V_a=0.13$ V (dot-dashed

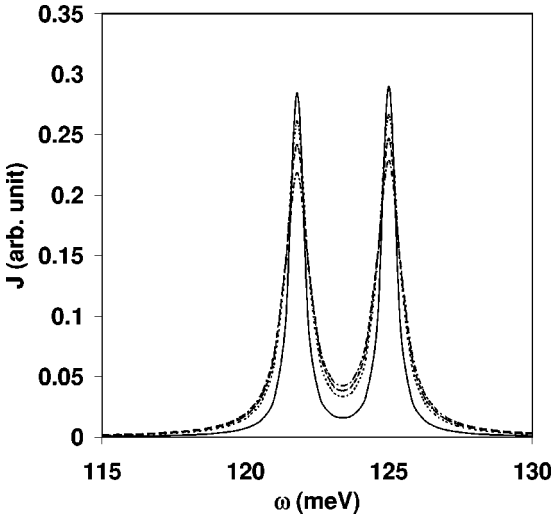


FIG. 7. Photocurrent as a function of frequency for various applied voltages: $V_a=0$ (solid line), $V_a=0.11$ V (dotted line), $V_a=0.12$ V (dashed line) and $V_a=0.13$ V (dot-dashed line). High doping case ($E_F=70$ meV) and $\Gamma_{2e}=0.1$ meV.

line)]. Because $N_1 \approx 0.5$ at all three applied voltages, the two peaks of the photocurrent spectrum have almost the same height. The most striking result is the presence of zero-bias photocurrent spectra caused by the asymmetric tunneling rates ($\Gamma_2^R = 0.1414 \gg \Gamma_2^L$).

## VI. SUMMARY

We have theoretically studied the tunneling current through the quantum dot with two energy levels irradiated by infrared light. The Anderson model for two discrete energy levels coupled with the electromagnetic field is used to simulate the system. The Keldysh Green function method is used to calculate the resonant photon-assisted tunneling current. This method is a convenient tool to include the electron correlation, which can not be ignored in QD's. Both the intralevel Coulomb interaction and the interlevel Coulomb interactions are found to be important. We have studied a realistic n-i-n self-assembled InGaAs/GaAs QDIP structure for both low doping ($E_F = 15$ meV) and high doping ($E_F = 70$ meV) cases. In both cases, the photocurrent is found to be a highly nonlinear function of the QD carrier density, in sharp contrast to that in QWIPs.

We find that the electron-electron interaction not only give rise to a Coulomb blockade on the dark current, but also leads to a double-peak photocurrent spectrum with an energy separation equal to the difference in the intralevel and interlevel Coulomb energies. In the high doping case, the Fermi level is above the QD ground state, and we obtain a sizeable zero-bias photocurrent, which is caused by the asymmetric tunneling rates of the conical QD. Because the dark current at zero bias (likely caused by the background raidation) is very small, we expect a high detectivity for this type of QDIP.

In this study, we have used resonant tunneling carriers as the source for photocurrent, in contrast to the captured carriers typically used in QWIPs and QDIPs.[24] Due to the phonon bottleneck effect,[10] it is predicted that the capture rate of electron by the QD will be low. This could reduce the performance of QDIPs, which use captured carriers as the scource for producing photocurrent. Using carriers injected via resonant tunneling process can avoid this problem.

## ACKNOWLEDGMENT

This work was supported by a subcontract from the University of Southern California under the MURI program, AFSOR, Contract No. F49620-98-1-0474.

[1] Y. Alhassid, Rev. Mod. Phys. **72**, 895 (2000).
[2] D. Goldhabar-Gordon, H. Shtrikman, D. Mahalu, D. Abusch-Magder, U. Meirav, and M. A. Kastner, Nature (London) **391**, 156 (1998).
[3] S. M. Cronenwett, T. H. Oosterkamp, and L. P. Kouwenhoven, Science **281**, 540 (1998).
[4] D. C. Ralph, C. T. Black, and M. Tinkham, Phys. Rev. Lett. **78**, 4087 (1997).
[5] D. M. T. Kuo and Y. C. Chang, Phys. Rev. B **61**, 11 051 (2000).
[6] D. M. T. Kuo, G. Y. Guo, and Y. C. Chang, Appl. Phys. Lett. **79**, 3851 (2001); D. M. T. Kuo, A. Fang, and Y. C. Chang, Infrared Phys. Technol. **42**, 433 (2001).
[7] S. Komiyama, O. Astafiev, V. Antonov, T. Kutsuwa, and H. Hirai, Nature (London) **403**, 405 (2000).
[8] Q. Xie, A. Kalburge, P. Chen, and A. Madhukar, IEEE Photonics Technol. Lett. **8**, 965 (1996).
[9] P. Recher, E. V. Sukhorukov, and D. Loss, Phys. Rev. Lett. **85**, 1962 (2000).
[10] J. Urayama, T. B. Norris, J. Singh, and P. Bhattacharya, Phys. Rev. Lett. **86**, 4930 (2001).
[11] A. P. Jauho, N. S. Wingreen, and Y. Meir, Phys. Rev. B **50**, 5528 (1994).
[12] H. Haug and A. P. Jauho, *Quantum Kinetics in Transport and Optics of Semiconductors* (Springer, Heidelberg, 1996).
[13] C. A. Stafford and N. S. Wingreen, Phys. Rev. Lett. **76**, 1916 (1996).
[14] Q. F. Sun, J. Wang, and T. H. Lin, Phys. Rev. B **58**, 13 007 (1998).
[15] Ph. Brune, C. Bruder, and H. Schoeller, Phys. Rev. B **56**, 4730 (1997).
[16] M. Holtaus and D. Hone, Phys. Rev. B **47**, 6499 (1993).
[17] S. Schmitt-Rink, D. S. Chemla, and H. Haug, Phys. Rev. B **37**, 941 (1988).
[18] P. Johansson and G. Wendin, Phys. Rev. B **46**, 1451 (1992).
[19] E. N. Bulgakov and A. F. Sadreev, J. Phys.: Condens. Matter **8**, 8869 (1996).
[20] J. Q. You and H. Z. Zheng, Phys. Rev. B **60**, 13 314 (1999).
[21] D. M. T. Kuo and Y. C. Chang, Phys. Rev. B **60**, 15 957 (1999).
[22] S. J. Xu, S. J. Chua, T. Mei, X. C. Wang, X. H. Zhang, G. Karunasiri, W. J. Fan, C. H. Wang, J. Jiang, S. Wang, and X. G. Xie, Appl. Phys. Lett. **73**, 3153 (1998).
[23] H. C. Liu, M. Buchanan, and Z. R. Wasilewski, Phys. Rev. B **44**, 1411 (1991).
[24] V. Ryzhii, Appl. Phys. Lett. **78**, 3346 (2001).
[25] Z. H. Chen, O. Baklenov, E. T. Kim, I. Mukhametzhanov, J. Tie, A. Madhukar, Z. Ye, and J. C. Campbell, Infrared Phys. Technol. **42**, 479 (2001).